A DIFFUSION EQUATION BASED ALGORITHM FOR DETERMINATION OF THE OPTIMAL NUMBER OF FIBERS USED FOR BREAST CANCER TREATMENT PLANNING IN PHOTODYNAMIC THERAPY

Ismael F.S.[1], **Amasha H.M.**[1, 2], **Bachir W.H.**[1, 3]
[1]Damascus University, Damascus, Syria
[2]Syrian Private University, Damascus, Syria
[3]Al-Sham Private University, Damascus, Syria

Abstract

It is essential in interstitial Photodynamic therapy (iPDT) treatment planning to ensure a homogeneous distribution within a tumor volume using cylindrical diffusing fibers while keeping the surrounding tissue intact. Light distribution is simulated through two algorithms based on the diffusion equation assuming diffusers as light sources. The first algorithm analyzes the diffusion equation and studies the effects of different variables (optical properties, delivered power, diffuser length, and position). Next, optical properties of breast were applied to estimate the volume that receives accepted light dose from one diffuser. In the second algorithm, multiple diffusers were simulated in order to find the relation between the volume and the number of required diffusers which are needed to cover cubical or cylindrical volume with sufficient light dose. Throughout this study, real values of optical properties, clinical laser power, and treatment time were considered to evaluate sufficient light doses. This study is in agreement with previous works in that optical properties are the major factors influencing light distribution in iPDT. It is shown that for a homogeneous phantom mimicking breast cancer and cubical or cylindrical shape, the number of required fibers N equal W×L or D^2 respectively.

Keywords: iPDT, diffusion equation, cylindrical diffuser fiber, sufficient light dose, breast cancer.

For citations: Ismael F.S., Amasha H.M., Bachir W.H. A diffusion equation based algorithm for determination of the optimal number of fibers used for breast cancer treatment planning in photodynamic therapy, *Biomedical Photonics*, 2019, vol. 8, no. 4, pp. 17–27. doi: 10.24931/2413–9432–2019–8–4–17–27

Contacts: Ismael F.S., e-mail: fatimah.esm@gmail.com

АЛГОРИТМ ОПРЕДЕЛЕНИЯ ОПТИМАЛЬНОГО ЧИСЛА ВОЛОКОН ИСПОЛЬЗУЕМЫХ ПРИ ВНУТРИТКАНЕВОЙ ФОТОДИНАМИЧЕСКОЙ ТЕРАПИИ РАКА МОЛОЧНОЙ ЖЕЛЕЗЫ НА ОСНОВАНИИ ДИФФУЗИОННОГО УРАВНЕНИЯ

Ismael F.S.[1], **Amasha H.M.**[1, 2], **Bachir W.H.**[1, 3]
[1]Университет Дамаска, Дамаск, Сирия
[2]Частный университет Сирии, Дамаск, Сирия
[3]Частный университет Аль-Шам, Дамаск, Сирия

Резюме

При планировании внутритканевой фотодинамической терапии (iPDT) с использованием цилиндрических диффузных волокон важно обеспечить однородное распределение света по всему объему опухоли, сохранив при этом целостность окружающей ткани. Авторы данной статьи смоделировали распределение света с помощью двух алгоритмов, основанных на уравнении диффузии, в которых в качестве источников света используются цилиндрические диффузоры. Первый алгоритм анализирует уравнение диффузии и изучает влияние различных переменных (оптических свойств источника, применяемой мощности, длины диффузора и его положения). Затем были использованы параметры оптических свойств молочной железы для оценки объема, который рассчитывает световую дозу от одного диффузора. Во втором алгоритме было смоделировано несколько рассеивателей для нахождения соотношения между объемом и количеством рассеивателей, необходимых для покрытия кубического или цилиндрического объема достаточной световой дозой. На протяжении всего этого исследования рассматривались реальные значения оптических свойств, клинической мощности лазера и времени лечения для оценки достаточных световых доз. Это исследование согласуется с предыдущими работами в том, что оптические свойства являются основными факторами, влияющими на распределение света

при iPDT. Показано, что, для однородного фантома, имитирующего рак молочной железы, кубической или цилиндрической формы, количество требуемых волокон N равно W×L или D^2, соответственно.

Ключевые слова: внутритканевая фотодинамическая терапия, уравнение диффузии, волокно с цилиндрическим диффузором, достаточная световая доза, рак молочной железы.

Для цитирования: Ismael F.S., Amasha H.M., Bachir W.H. A diffusion equation based algorithm for determination of the optimal number of fibers used for breast cancer treatment planning in photodynamic therapy // Biomedical Photonics. – 2019. – Т. 8, № 4. – С. 17–27. doi: 10.24931/2413–9432– 2019–8–4–17–27

Контакты: Ismael F.S., e-mail: fatimah.esm@gmail.com

Introduction

Photodynamic therapy (PDT) combines a light sensitive compound (photosensitizer) with light to generate reactive oxygen species, which, in sufficient quantities, lead to tissue destruction [1]. The development of photoactive compounds that absorb light at longer wavelengths, with greater penetration in tissue, has led to the development of treatments for larger, deep-seated tumors [2].

The diffusion approximation to modeling light transport works well for biological tissues at near-infrared PDT treatment wavelengths, where light scattering dominates over absorption. In addition, numerical solution of the diffusion equation, as used here, allow for the modeling of light transport in systems with time frames that are feasible for clinical application. Also, diffusion theory enables quick estimation of the fluence rate distribution in a homogeneous medium [3].

Recently, computer simulations suggested that cylindrical diffusing fibers (CDFs) are more effective than flat-cut fibers in delivering the therapeutic light in iPDT especially for bulky tumors [4, 5]. B. Farina et al. [6] simulated cylindrical diffuser as linear array of ideal point sources to extract fluence rate distribution in hollow organ. Baran and Foster [7] used GPU for simulation. They modeled the diffuser based on TiO_2 particles. This model predicts a fluence distribution similar to that modeled by B Farina et al. They compared the radial degradation of fluence from the diffuser for both models and demonstrated that a model based on a linear of point sources is sufficient for determining fluence distribution. Baran and Foster in Ref [5], used the same diffuser modeled by them to make comparison between numbers of cylindrical diffusing fibers and flat cleaved ones.

A number of research groups have focused their efforts on optimizing the fiber placements. T.M. Baran et al. [5] demonstrated optimization of six CDFs positions in order to create treatment plans for iPDT of (6.1×7.5×7 cm) in brain. M.D. Altschuler et al. [8] used twelve CDFs in (2.5×3×5 cm). E. Oakley et al. [9] also demonstrated a treatment plan using finite element method and eleven CDFs to deliver an accepted light dose to (5×4×4 cm) in head and neck cancer. Those studies did not indicate to the ability of single CDF to deliver accepted light doses around it. In the current study, benefits from analyzing the diffusion equation were taken to determine the whole volume with optical properties of breast cancer that has accepted light dose of all its points. This simulation study contains two codes which are regarded as important prior steps for practical procedure that we are planning to do in the laboratory. First code provides programming description of single CDF using diffusion equation. Four available CDFs in the laboratory were simulated in the second code. Results of this study clarifies interaction between external laser power, CDF length and medium optical properties and how it could be useful to determine the required number and full length of fiber tip to cover full volume with suitable fluence rate.

Materials and Methods

Tissue model and software algorithm

Following diagrammatic analysis of equation 2 assumes a cube (5^3 cm^3), divided into fractional (0.5^3 cm^3) cubes, fractional cubes could be smaller if requested. CDF position is the central cube (x, y, z) = (2.5, 2.5, 5). While assuming that the decrement of CDF length starts from the top surface of the cube, the coordinate (z) must be equal to the full length of the corresponding cube. Figure 1 represents the tissue model. The core of the PDT treatment planning simulation is the calculation of the light intensity (fluence rate) distribution in tissue generated by a CDF. Therefore, first code is made as flexible as to calculate the fluence rate $\varphi(r)$ as a function of each variable (h, l, s, μ_{eff}, μ_a) independently in every point (pixel) in the cube. The second code allows choosing CDFs number (maximum is four). In addition to changing l, s, μ_{eff}, μ_a, t, *volume* and *distance between pixels*. Figure 2 displays the schematic of the codes. The light distribution, diffusion equation and tissue model were modeled in Matlab (2016a).

Throughout the paper, each observing point receives N rays. N represents the number of source points along the CDF. The points located at equal distances away from

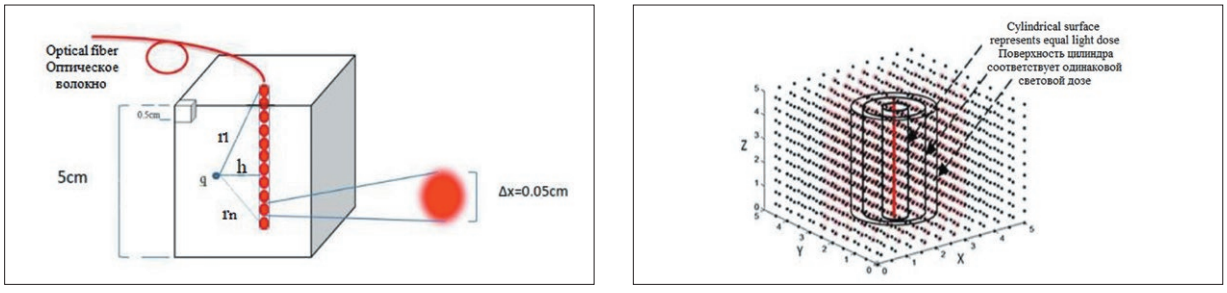

a b

Fig. 1.
a – Cube, fractional cubes, CDF, point source and observing points are the components of the tissue model. Each point receives N rays. N is the number of total source points along the CDF (Dimensions are for clarification and they are not no scale);
b – Cylindrical surfaces represent points that have equal fluence rate

Рис. 1.
a – Куб, дробные кубы, оптическое волокно с цилиндрическим диффузором (CDF), точечный источник и точки наблюдения являются компонентами модели ткани. Каждая точка получает N лучей. N – это общее количество точек-источников вдоль CDF (размеры даны для пояснения, и они не в масштабе);
b – Цилиндрические поверхности представляют точки с одинаковой скоростью потока

CDF receive equal light dose and form a cylindrical surface around CDF (fig. 1b).

Laser treatment fiber

This study provides profiling of optical fiber which is made from RD-ML50 (Medlight S.A, Switzerland). Treatment fiber specifications are as follows: transmission of 630–760 nm, overall diameter 1 mm, illumination length of 50 mm, maximum (CW) power density (in air) of 0.5 W/cm, absolute maximum input power of 2.0 W (CW). Treatment regions: breast, prostate, brain, heart, lung and diaphragm. The diffuser length is 5 cm or less (in increments of 0.5 cm); density power, W/cm and energy, J/cm were specified for each fiber) [10].

Diffusion theory

Cylindrical diffusor fiber was modeled in two geometries. Two equations can be found in the literature that estimate the fluence rate emitted from a light source of a length l in heterogeneous/homogeneous media (equations 1 and 2). Equation 1 discretizes the diffusing part of the optical fiber as a sum of several point light sources [11–13]. Equation 2 considers the whole fiber as a finite line light source with 2D cylindrical light emission characteristics [14]. The first equation 1 is considered as complex equation to estimate the fluence rate, on the basis that the calculation of the fluence rate at a distance r from the fiber is the sum of each light source contribution. Whereas equation 2 computes the fluence rate values using the minimal distance r from the fiber.

$$\varphi(r) = \frac{3\, s\, l\, \mu_s'}{4\pi} \cdot \frac{1}{N-1} \cdot \sum_{i=1}^{N} \frac{e^{-\mu_{eff}\, r_i}}{r_i} \quad (1)$$

$$\varphi(r) = P\sqrt{\frac{2\delta}{\pi r}} \cdot \frac{e^{-r/\delta}}{2\pi \cdot \mu_a \cdot \delta^2} \quad (2)$$

Where P is power of one point, $D = \frac{1}{3\,(\mu_a + \mu_s')}$, δ is the optical penetration depth in m and is equal to $\sqrt{D/\mu_a}$, s is the power of the point source in mW/cm; $\varphi(r)$ is the fluence rate in mW/cm; the quantity $\mu_{eff} = \sqrt{(3 \cdot \mu_a \cdot (\mu_a + \mu_s'))}$ is the effective attenuation coefficient in tissues. The differential $\Delta x = l/(N-1)$ is the length of the elemental (discretized) source segment. The odd integer N is the number of points used in the summation over the source, with one point always placed in the middle of the CDF. The distance between the i_{th} point of the linear light source and the observing point is $r_i = \sqrt{x_i^2 + h^2}$, where $x_i = [(i-1-(N-1)/2) \cdot \Delta x]$ is the cylindrical coordinate along the fiber from the center of the linear source. h is the distance between the observing point and the fiber axis as it is shown in fig. 1a. The numerical value of the summation should be independent of N (or Δx) if N is large enough. Accurate results of the summation can be obtained if Δx = 0.05 cm. In this study, summing N = 101 is available [8, 15]. Obviously, equation 2 is simpler than 1. Depending on geometrical optics equation 1 could be regarded as more accurate method than the equation 2. That is why fluence rate is estimated using the equation 1 throughout this study. For simplicity, we use the light fluence (fluence rate × exposure time) for the PDT dose throughout the paper. The illumination time, through this study, was not fixed (300 sec in the first algorithm and 150 sec in the second algorithm). Final light dose at each point is the summing of light doses that were received from all diffusers. Specifically, tissue necrosis occurs above a threshold light dose [16]. The higher threshold of target dose is determined by minimizing damage to surrounding tissue. To make this study closer to reality, thresholds light dose are assumed to be 20–50 J/cm^2 and 90–300 J/cm^2 with optical properties of breast and prostate cancer, respectively [8, 17].

Optical properties of the studied tissues and patient's prostate

Optical properties at 732 nm in human prostate before and after PDT are taken from Altschuler et al. [8] and listed in table 1. While Optical properties of heart, breast,

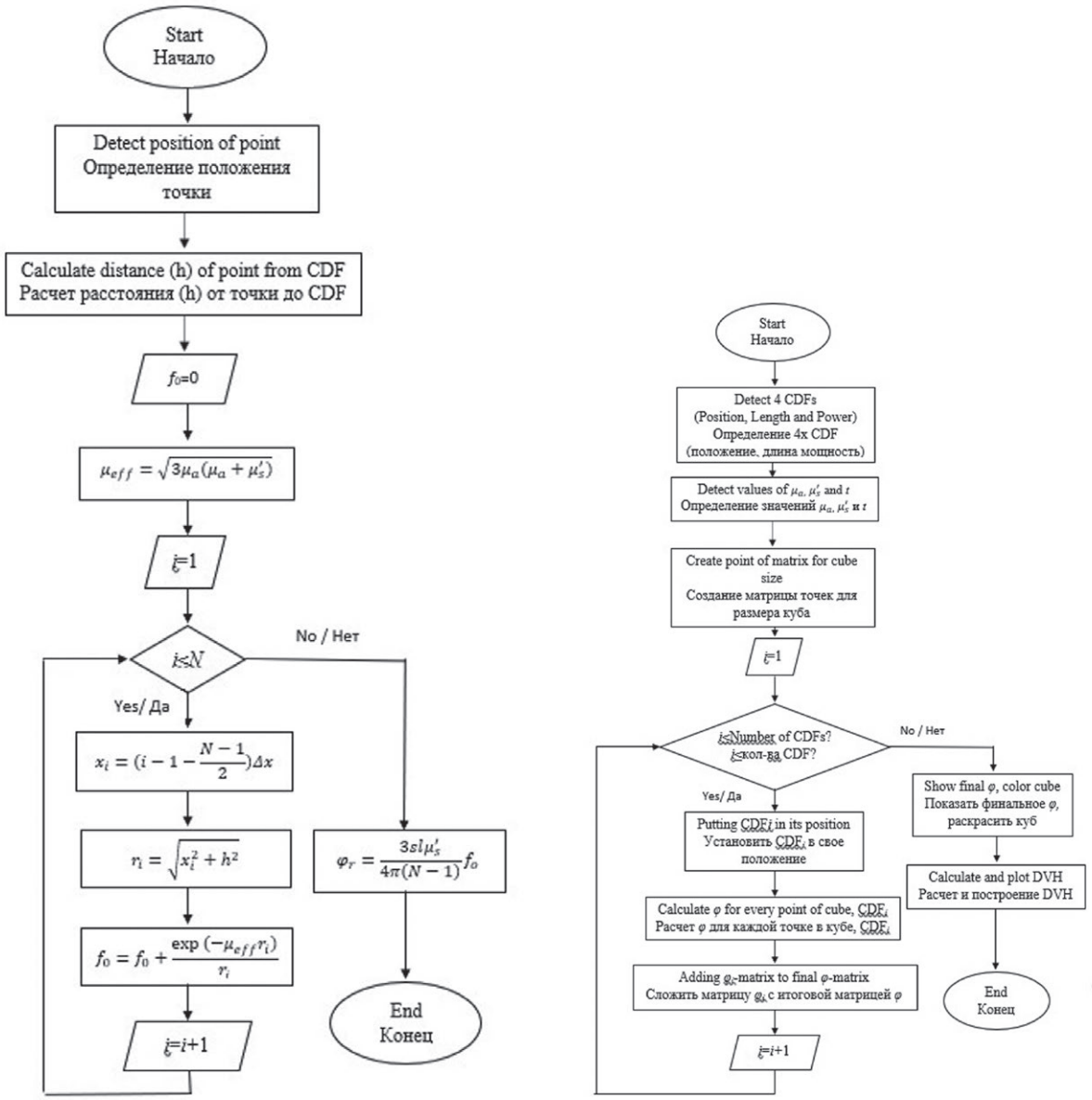

a b

Fig. 2. The block diagram illustrating two software planning algorithms:
a – Algorithm code for analyzing diffusion theory and CDF specification;
b – Algorithm code to calculate total fluence light and plotting color cube and Dose Volume Histogram (DVH)
Рис. 2. Блок-схема, иллюстрирующая два алгоритма программы:
a – Алгоритм кода для анализа теории диффузии и спецификации цилиндрических диффузоров (CDF);
b – Алгоритм кода для расчета общей плотности света и построения цветового куба и гистограммы доза-объем (DVH)

Table 1
Optical properties at 732 nm in human prostate gland (before and after PDT) for patient number 3 and 5 [8]
Таблица 1
Оптические свойства предстательной железы (до и после ФДТ) для 732 нм пациентов 3 и 5 [8]

Patient Number Номер пациента	Before PDT До ФДТ		After PDT После ФДТ	
	μ_a, cm^{-1}	μ_s', cm^{-1}	μ_a,	μ_s', cm^{-1}
3	0.15	22.0	0.07	33.4
5	0.21	11.8	0.13	7.18

Table 2
Optical properties of human heart, breast, lung, diaphragm tissues [11]
Таблица 2
Оптические свойства тканей сердца, молочной железы, легких, диафрагмы человека [11]

Tissue Ткань	λ,nm	μ_a, cm^{-1}	Average Усредненное	μ_s', cm^{-1}	Average Усредненное
Heart Сердце	661	[0.18–0.12]	0.15	[5.22–90.80]	48
Breast (normal) Молочная железа (норма)	660	[0.037–0.11]	0.074	[11.4–13.5]	12.45
Breast (tumor) Молочная железа (опухоль)	690	[0.07–0.1]	0.085	[14.7–17.3]	16
Lung Легкое	661	[0.49–0.88]	0.68	[21.14–22.52]	21.83
Diaphragm Диафрагма	661	[0.15–1.08]	0.62	[9.65–21.7]	15.7

lung, diaphragm tissues are taken from Julia J.L. Sandell and T.C. Zhu review [11] and given in table 2.

Results and discussion

The present study was independent of allowed illumination/dark time or oxygen consumption. Each factor in equation 1 has a different effect. Throughout this part increment in distance is 0.125 cm. Illumination treatment time is 5 min. Source power is 0.5 mW/cm. The following disscution presents four effects.

Distance perpendicular to the fiber axis (h)

Figure 3*a* shows the variation of calculated light fluence distribution for different distances in the same prostate gland (optical properties are taken from table 1). The average optical properties were very different between the upper and lower line. The light fluence rate at 0.5 cm far away from the CDF varied from 64.59 J/cm^2 (before PDT) to 30.5 J/cm^2 (after PDT). Significant change of optical properties was observed before and after PDT treatment in the same patient number 3. Figure 3*b* shows the variation of calculated light fluence distribution for different distances in heart, breast, lung and diaphragm (optical properties are mentioned in the table 2). As a result, closed values of fluence rate were observed when optical properties approximately the same (of lung and diaphragm). Absorption coefficient of breast is the smallest, so it allows higher distribution light (φ=50 J/cm^2 at 0.5 cm away from CDF). From figure 3*b*; the values of φ are 50 J/cm^2 at 0.375 cm for heart, and 50 J/cm^2 at 0.5 cm for breast. Thus, practically two CDFs are required to deliver 100 J/cm^2 for points at those distances. In contrast, for lung or diaphragm two CDFs deliver accepted fluence rate 90 J/cm^2 at 0.125 cm only. More explanation is provided in following absorption and scattering coefficients effects.

Absorption and scattering coefficients effects

Remarkable advances were made in the last two decades to determine the *in vivo* optical properties in humans in a variety of organs. The absorption coefficient varies largely over the visible spectrum, while the scattering coefficient of tissue decreases monotonically as the wavelength increases [18]. The presence of chromophores affects the absorption coefficient. Although the actual range of the *in vivo* optical properties is tissue type dependent, generally varied in the ranges μ_a =0.03–1.6 cm^{-1} and μ_s'=1.2–40 cm^{-1} [11]. Since equation 1 is a nonlinear equation of two parameters μ_a and μ_s', it was very difficult to separate effects of μ_s' and μ_a from

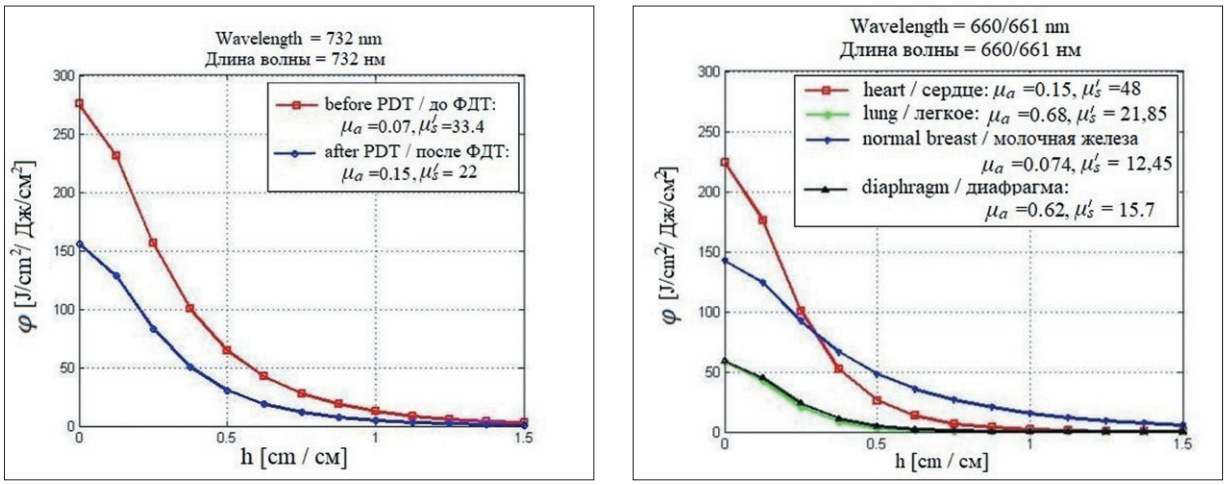

a b

Fig. 3. Fluence rate curve plotted at different distances:
a – in prostate gland;
b – for other organs
Рис. 3. Кривая светового потока на разных расстояниях:
a – в предстательной железе;
b – для других органов

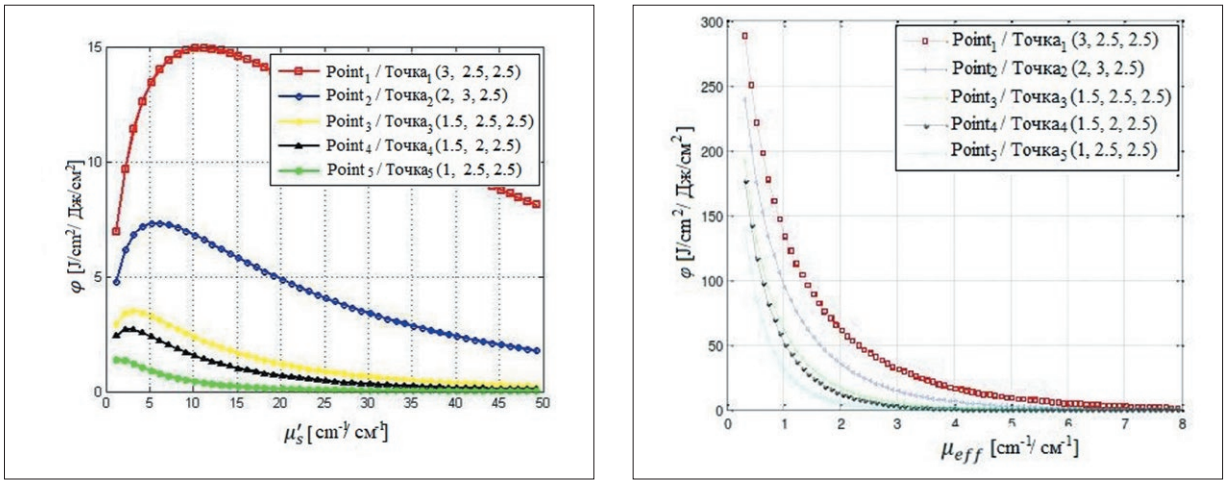

a b

Fig. 4. The dependence of light fluence rate at different points from:
a – μ_s' ;
b – μ_{eff}
Рис. 4. Зависимость интенсивности светового потока в разных точках от:
a – μ_s' ;
b – μ_{eff}

each other. Now, the studied medium is supposed to be heterogeneous, and five observing points are considered. Therefore, to understand the effective attenuation coefficient effect, it is required to fix μ_s' at 20.6 cm^{-1} (is the average of its range) and μ_{eff} is changing along 0.33–14.13 cm^{-1}. We used these values to understand the expected standard behavior of optical properties, and to anticipate the variation in tissue constitution that yields the tissue optical properties at any desired wavelength [19].

In the opposite case, μ_s' is changed along its range and μ_{eff} is fixed at value (7.23 cm^{-1}); the average of its range. To explain μ_{eff} and μ_s' effects, five observing points were taken at the distances (h1=0.5, h2=0.7, h3=1, h4=1.12, h5=1.5) cm away from CDF. These five points represent

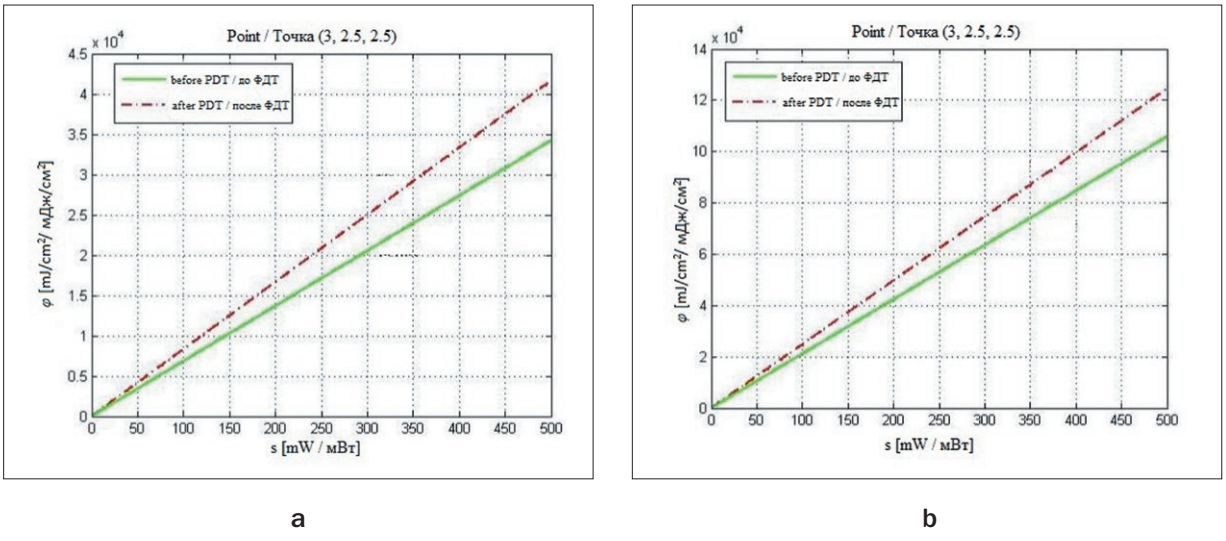

Fig. 5. Fluence rate as a function of power density s:
a – Before PDT: μ_s'=11.8 cm^{-1}, μ_a=0.21 cm^{-1}; after PDT: μ_s'=7.18 cm^{-1}, μ_a=0.13 cm^{-1}
b – Before PDT: μ_s' =22 cm^{-1}, μ_a=0.15 cm^{-1}; after PDT: μ_s'=33.4 cm^{-1}, μ_a=0.07 cm^{-1}

Рис. 5. Интенсивность оптического потока как функция плотности мощности s:
a – До ФДТ: μ_s' =11.8 см$^{-1}$, μ_a=0.21 см$^{-1}$; после ФДТ: μ_s'=7.18 см$^{-1}$, μ_a=0.13 см$^{-1}$
b – До ФДТ μ_s'=22 см$^{-1}$, μ_a=0.15 см$^{-1}$; после ФДТ: μ_s'=33.4 см$^{-1}$, μ_a=0.07 см$^{-1}$

the nearest five cylindrical surfaces. Figure 4 shows the relationship between the light fluence rate and the optical properties.

Figure 4*a* shows that the fluence rate (for point 1) rapidly increases between 1.2 and 10 cm^{-1}, then approximately fixed between 10 and 15 cm^{-1}. As a result, reduced scattering coefficient does not cause increase in fluence rate after value 10 cm^{-1}. For point 2, decline in fluence rate occurs after 7 cm^{-1}. Although the difference in distance is only 2 mm between point 1 and 2, there is a large difference in fluence rate between them. For other points higher values of fluence rate are along 1.2–5 cm^{-1}. As a result, in experimental phantom, for higher distances, it is good to make μ_s'≤ ~10 cm^{-1}. For larger distances (0.7, 1, 1.12, 1.5 cm), it is better to make μ_s' ~ 5, 3.2, 3.2, 1.2 cm^{-1}, respectively. Figure 4b shows the relationship between the light fluence rate and the effective attenuation coefficient as exponential decay curves. As shown in figure, it is clear that values corresponding to point 1 (0.5 cm) have higher fluence rate values, while lower lines represent other points respectively. For $\varphi(r)$ that was lower than 90 J/cm^2; μ_{eff} is 1.53 cm^{-1} for h_1. For other points μ_{eff} was 1, 0.73, 0.6, 0.5 cm^{-1}, respectively. Two algorithms allow to change ranges and values of μ_s' and μ_{eff} to get accepted light dose and could be useful in preparing phantoms at laboratories. As a result, knowledge of optical properties of tissues is of great importance for interpretation and quantification of the diagnostic data. Fluence rate at virtual diffuser points depends on optical properties of studied medium. It was ~87.7 J/cm^2 with prostate optical properties μ_s' =14.3, μ_a =0.3 cm^{-1}. While it became 199.5 J/cm^2 when μ_a decreases by ten times. It is well known that absorption coefficient is included in μ_{eff} expression. From our findings and for the optical properties of all biological tissues studied in ref. [11], it was found that the absorption coefficient μ_a has a more significant influence on light fluence rate distribution than reduced scattering coefficient μ_s'. It is noteworthy to say that our results are valid for wavelength range 600–800 nm at certain wavelengths of human tissues that was also mentioned in ref. [11].

Power density effects (s)

Source catheters are used for both light delivery and measurement of optical properties. Usually, the light dose is given in terms of external power density delivered by the light system. As it is noted in fiber specifications, *s* is 0.5 mW/cm at maximum allowed input power 2W. The power is considered to be 0.5 mW/cm through all previous study. Consequently, power of full diffuser length is 2.5 W. Maximum power density (in air) is 500 mW/cm (CW) as mentioned in the technical specifications of Medlight CDFs [10], so the power is varied between 0 and 500 mW/cm through the two codes. Optical properties of patients were taken from ref. [8]. As can be seen in figure 5*a*, optical properties of patient number 5 were μ_s' =11.8 cm^{-1}, μ_a =0.21 cm^{-1} (before PDT). After PDT, the values changed to μ_s'=7.18 cm^{-1}, μ_a =0.13 cm^{-1}. Fluence rate became larger after PDT [8].

Figure 5*b* shows linear relationship between *s* and $\varphi(r)$ that to deliver accepted fluence rate 90 J/cm^2, applied power should equal at least ~432 mW/cm, while after PDT it decreased to 369 mW/cm. If *s* is limited at 250, flu-

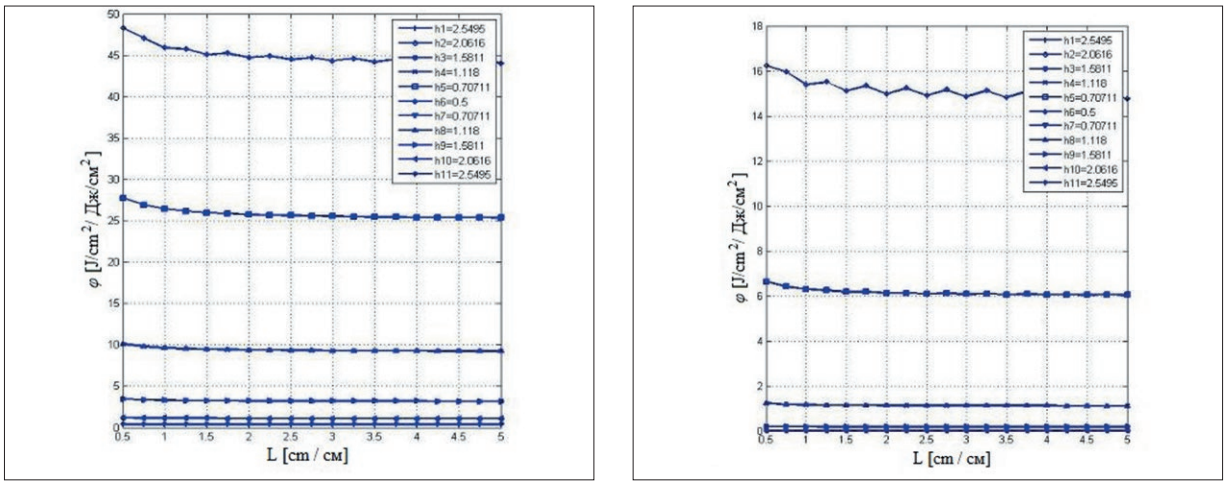

a b

Fig. 6. Fluence rate as function of diffuser length *L*. s = 0.5 mW/cm, μ_s' = 14 cm^{-1}, *t* = 5 min:
a – μ_a=0.09 cm^{-1}
b – μ_a=0.3 cm^{-1}
Рис. 6. Интенсивность оптического потока как функция длины диффузора *L*. s=0.5 мВт/см, μ_s' = 14 см$^{-1}$, *t* = 5 мин.
a – μ_a=0.09 см$^{-1}$
b – μ_a=0.3 см$^{-1}$

ence rate is 50 J/cm^2 (before) and 61.5 (after). It was clear that fluence rate became higher after the PDT. Results for patients 2, 4, 12 and 9 [8] confirm that μ_a has a significant effect on light fluence rate distribution.

Cylindrical diffuser length effect

Returning to equation 1; the fluence rate clearly appears proportional to the tip length. Increasing the fluence rate is related to the density of number of source points over the diffuser (N). As a result, the fluence rate at certain point is not affected by varying tip length. This result is illustrated by figure 6.

Figure 6 shows the relationship between φ and *L*. The CDF was positioned at cube center, each line represented two opposite distances. Distances furthest from CDF were shown in small rectangle. As it was expected, light fluence rate was not affected by increasing length, for similar inputs and distances, but if μ_a is changed to 0.3 cm^{-1}, then fluence rate will decrease to about 15 J/cm^2 at h6=0.5 cm while it is about 45 J/cm^2 with μ_a=0.09 cm^{-1}.

Clearly there is a big difference between $\varphi(h6)$ and $\varphi(h5)$. As a result, there is major attenuation in fluence rate as distance increases.

Fluence rate calculations were done using basic diffusion equation (eq. 1). As it is well known, the generating of matrixes in order to calculate fluence rate at each point is a cumbersome procedure. Conditions were determined to accept fluence rate. This condition could be changed as required for a given tissue, photosensitizer or wavelength. Our results agreed with prior works where optical properties have considerable effect on light distribution in any given medium [11]. However, in real clinical producers, CDF length cannot be changed and practically, due to fixed distances between slots used for guiding PDT fibers inside the tissue which equal 0.5 cm on average [8], distance between tow CDFs could not be less than 0.5 cm.

Volume versus number of CDFs

Actual input parameters had been taken into following consideration. Optical properties of breast cancer are μ_a = 0.085 cm^{-1}, μ_s' = 16 cm^{-1} [11]. First algorithm is used to

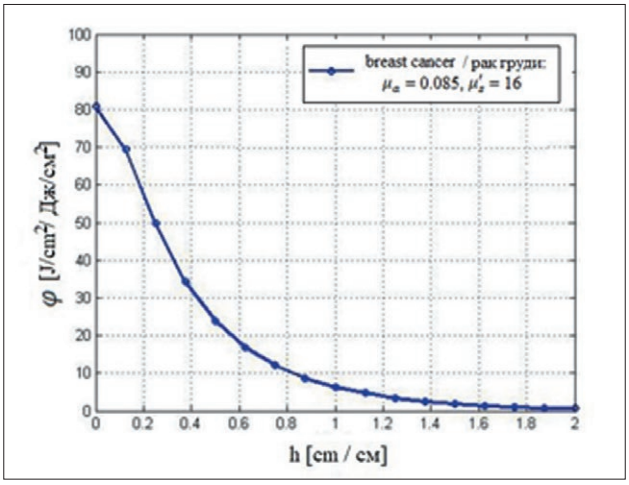

Fig. 7. Fluence rate is as a function of distance for breast cancer tissue. Input parameters are: s=50 mW/cm, t=150 sec. Light dose at h=0.5 cm is 24 J/cm^2 for breast
Fig. 7. Интенсивность светового потока как функция расстояния для ткани рака молочной железы. Входные параметры: *s*=50 мВт/см, *t*=150 сек. Световая доза при *h*=0.5 cm равна 24 Дж/см^2 для молочной железы

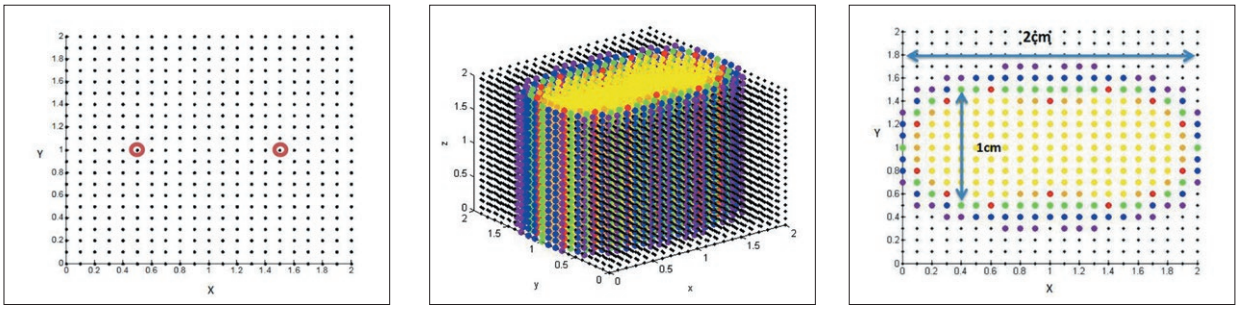

Рис. 8. Light distribution resulted from two CDFs with s = 50 mW/cm, *t* = 150 sec, μ_a = 0.085 cm^{-1}, μ_s' = 16 cm^{-1}:
a – Top-down view shows positions of CDFs placed at (0.5, 1, 2), (1.5, 1, 2);
b – Yellow points have accepted dose and form volume 1x2x2 cm;
c – Top-down view of cube after light distribution: light dose in red points is less than 20 J/cm^2 and more than 15 J/cm^2, green points represent pixels which have dose that is less than 15 J/cm^2 and more than 10 J/cm^2, blue/ violet points have the dose that is less than 10 J/cm^2

Рис. 8. Распределение света, полученное при использовании двух CDF при s = 50 мВт/см, t = 150 с, μ_a = 0,085 см$^{-1}$, μ_s' = 16 см$^{-1}$:
a – Положение CDF, размещенных в точках (0.5, 1, 2), (1.5, 1, 2) (вид сверху);
b – Желтым цветом выделены точки, получившие необходимую световую дозу. Их объем составляет 1x2x2 см.
c – Распределение света (вид сверху): доза света в красных точках составляет менее 20 Дж/см^2 и более 15 Дж/см^2, зеленые точки представляют пиксели с дозой менее 15 Дж/см^2 и более 10 Дж/см^2, синие/фиолетовые точки имеют дозу менее 10 Дж/см^2

estimate fluence rate along 2.5 cm far away from single CDF (full length of tip is 5 cm) is placed at center of cube (5×5×5 cm). Initial position of CDF is (x=2.5 cm, y=2.5 cm, z=5 cm); since x, y can be changed along X and Y axes from 0.5 cm to 5 cm, while z must be set at the full length of CDF.

Figure 7 shows that sufficient light dose is reached for approximately 0.25–0.5 cm around CDF. Higher threshold of 50 J/cm^2 is exceeded at h $\leq$ 0.25 cm. As a result, for optical properties of breast cancer, accepted light dose reaches to volume of one cylinder with full diameter of D = 1 cm. Figure 8 is the result of second algorithm. Figure 8*a* shows two CDFs in a line. As can be seen from figure 8*a*, two CDFs can cover two centimeters in one direction of volume. While approximately only one centimeter in the vertical orientation could be covered with light dose of 20–50 J/cm^2.

Length of CDFs must be near the height of the volume. For the breast cancer tissue, the covered volume equals approximately 1×N×L (cm) as represented in figure 8c. N is the number of CDFs, L is the length of diffusers. The volume (with accepted light dose) is 1×2×2=4 cm^3. To cover full cube size which is 2×2×2 (cm), four CDFs must be placed at (0.5, 0.5, 2), (0.5, 1.5, 2), (1.5, 1.5, 2), (1.5, 0.5, 2) (fig. 9*a*). The maximum covered volume with accepted light dose equals four times of cylinder c1 (cylinder c1 is indicated in figure 9*b*).

It can be concluded that for delivering sufficient light dose (20–50 J/cm^2) to any phantom which has cuboid or cylindrical shape and has optical properties of breast cancer, it is needed to place (W×L) or (D^2) CDFs respectively with distance (1 cm) between each two CDFs. Where, W, L are the rectangular sides and D is the cylinder diameter. Practically, optimization theories are applied to optimize places of a lower number of CDFs [5, 8]. Finding an algorithm to choose suitable powers represents another practical solution to reduce required fibers.

Dose-volume histogram

A DVH, more properly called a cumulative dose volume histogram, expresses the percentage of an organ that has received more than a given dose [20]. It is useful to summarize the volumetric distribution of light doses. Second code allows plotting DVH (fig. 9*c*) that corresponds to figure 9*b*. For higher accuracy; distance between pixels has been reduced to 0.05 cm. Consequently, number of slices is 40 slices (2/0.05 cm); total considered points are 40×40×number of slices. Plotting the prism with finer voxels causes much longer time to get φ_{total} matrix (final fluence rates resulting from four CDFs), while the time needed to calculate the DVH is only a second or so because no feasibility procedures are involved. Using DVH, it is possible to estimate percentage of points which accumulated sufficient light doses. With optical properties of breast cancer, sufficient light doses are attained in more than 95% of all cube points. Figure 9*c* shows DVH. Another case is studied with optical properties of brain cancer (μ_a = 0.2 cm^{-1}, μ_s' = 5 cm^{-1}) [5] (all other inputs are fixed). Results indicate that percentage of the covered volume with accepted light dose is reduced to 10% of the number of pixels with brain cancer (μ_a = 0.2 cm^{-1}, μ_s' = 5 cm^{-1}). Low level of percent coverage imposes using much more CDFs. T.M. Baran and

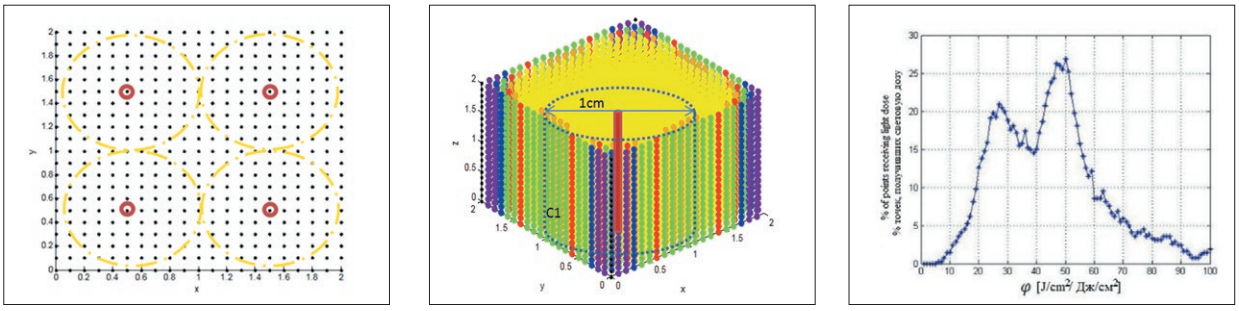

a b c

Рис. 9. Light distribution from four CDFs with *s* = 50 mW/cm, *t* = 150 sec, μ_a = 0.085 cm^{-1}, μ_s' = 16 cm^{-1}:
a – Four CDFs placed at (0.5, 0.5, 2), (0.5, 1.5, 2), (1.5, 1.5, 2), (1.5, 0.5, 2);
b – The distributed light forms a volume that is approximately 2x2x2 cm. Colors are the same as in figure 8;
c – The Dose-volume histogram for the results of four CDFs with 40x40x40 pixels. The vertical axis is the percent of total pixels that receive light doses. Summing the number of points showed that more than 63000 pixels out of 64000 received sufficient light dose

Рис. 9. Распределение света, полученное при использовании четырех CDF при *s* = 50 мВт/см, *t* = 150 с, μ_a = 0,085 см$^{-1}$, μ_s' = 16 см$^{-1}$:
a – Положение четырех CDF, размещенных в точках (0,5, 0,5, 2), (0,5, 1,5, 2), (1,5, 1,5, 2), (1,5, 0,5, 2);
b – Распределение света образует объем, который составляет примерно 2x2x2 см. Цвета такие же, как на рисунке 8.
c – Гистограмма «Объем-доза» для результатов четырех CDF с 40x40x40 пикселей. Вертикальная ось – процент от общего количества пикселей, которые получают световые дозы. Суммирование общего количества пикселей показало, что более 63000 пикселей из 64000 получили достаточную световую дозу

T.H. Foster et al. [7] used eight CDFs to deliver 2270–2350 J (333–1178 J/cm^2) to accumulate 90 J/cm^2 in 90% of tumor volume that was 5 cm^3 approximately. By raising the delivered power (*s*) or time treatment the percentage of coverage rises as well. In this regard, consumption of oxygen and the kind of photosensitizer must be considered in *in vivo* studies according to the treated organ.

Conclusion

This study is considered as the first inclusive description of cylindrical diffuser fibers using basic equation of diffusion theory (eq. 1). It was found that optical properties and distance away from CDF had the major effects on light distribution. For light absorbing media (i.e. prostate) which is virtually made of blood, high power is required in order to attain adequate light distribution in the tissue. On the other hand, for highly scattering media such as breast tissue, increasing the number of CDF fibers with lower power is highly recommended to avoid thermal collateral damage. Moreover, the study provides a guideline for proper localization of optical detectors inside tissue for investigating fluorescence during PDT. In addition, this simulation was very accurate in calculating the light doses at each point because of small size of voxels. Using specific colors for each range of light dose allowed estimating the whole volume covered by the sufficient light dose without referring to the matrixes. This simulation would be flexible regarding changes in variables in equation 1 including time, distance between points and the size of volume structure.

ЛИТЕРАТУРА

1. Dougherty T.J., Gomer C.J., Henderson B.W., Jori G., Kessel D., Korbelik M., Moan J., Peng Q. Photodynamic therapy // J Natl Cancer Inst. – 1998. – Vol. 90(12). – P. 889–905.
2. Wilson B.C., Patterson M.S., Lilge L. Implicit and explicit dosimetry in photodynamic therapy: a New paradigm // Lasers Med Sci. – 1997. – Vol. 12(3). – P. 182–99.
3. Haskell R.C., Svaasand L.O., Tsay T.T. et al., Boundary conditions for the diffusion equation in radiative transfer // Journal of the Optical Society of America A. – 1994. – Vol. 11(10). – P. 2727–2741.
4. Shafirstein G., Bellnier D., Oakley E., et al. Interstitial Photodynamic Therapy—A Focused Review // Cancers. – 2017. – Vol. 9(2). – E12. doi:10.3390/cancers9020012.

REFERENCES

1. Dougherty T.J., Gomer C.J., Henderson B.W., Jori G., Kessel D., Korbelik M., Moan J., Peng Q. Photodynamic therapy, *J Natl Cancer Inst*, 1998, vol. 90(12), pp. 889–905.
2. Wilson B.C., Patterson M.S., Lilge L. Implicit and explicit dosimetry in photodynamic therapy: a New paradigm, *Lasers Med Sci*, 1997, vol. 12(3), pp. 182–99.
3. Haskell, R.C., Svaasand L.O., Tsay T.T., Feng T.C., McAdams M.S., Tromberg B.J. Boundary conditions for the diffusion equation in radiative transfer, *Journal of the Optical Society of America A*, 1994, vol. 11(10), pp. 2727–2741.
4. Shafirstein G., Bellnier D., Oakley E., Hamilton S., Beeson K., Parilov E., Potasek M. Interstitial Photodynamic Therapy—A Focused Review, *Cancers*, 2017. – vol. 9(2), e12. doi:10.3390/cancers9020012.

5. Baran T.M., Foster T.H. Comparison of flat cleaved and cylindrical diffusing fibers as treatment sources for interstitial photodynamic therapy // Med. Phys. – 2014. – Vol. 41(2). – 022701. doi: 10.1118/1.4862078.
6. Farina B., Saponaro S., Pignoli E., Tomatis S., Marchesini R. Monte Carlo simulation of light fluence in tissue in a cylindrical diffusing fiber geometry // Phys Med Biol. – 1999. – Vol. 44(1). – P. 1–11.
7. Baran T.M., Foster T.H. New Monte Carlo model of cylindrical diffusing fibers illustrates axially heterogeneous fluorescence detection: simulation and experimental validation // J Biomed Opt. – 2011. – Vol. 16(8). – 085003. doi: 10.1117/1.3613920.
8. Altschuler M.D., Zhu T.C., Li J., Hahn S.M. Optimized interstitial PDT prostate treatment planning with the Cimmino feasibility algorithm // Med. Phys. – 2005. – Vol. 32. – P. 3524–3536.
9. Oakley E., Bellnier D.A., Hutson A., et al. Surface Markers for Guiding Cylindrical Diffuser Fiber Insertion in Interstitial Photodynamic Therapy of Head and Neck Cancer // Lasers Surg Med. – 2017. – Vol. 49(6). – P. 599–608.
10. Cylindrical light diffuser Model RD. Available at: http://www.medlight.com/pdf/Doc_RD_0801E.pdf. (accessed 28.11.2019)
11. Sandell J.L., Zhu T.C. A review of in-vivo optical properties of human tissues and its impact on PDT //Journal of Biophotonics. – 2011. – Vol. 4(11–12). – P. 773–87.
12. Dimofte A., Finlay J.C., Liang X., Zhu T.C. Determination of optical properties in heterogeneous turbid media using a cylindrical diffusing fiber //Physics in Medicine and Biology. – 2012. – Vol. 57(19). – P. 6025–46.
13. Dimofte A., Finlay J.C., Zhu T.C. A method for determination of the absorption and scattering properties interstitially in turbid media // Physics in Medicine and Biology. – 2005. – Vol. 50(10). – P. 2291–311.
14. Jacques S.L., Pogue B.W. Tutorial on diffuse light transport // Journal of Biomedical Optics. – 2008. – Vol. 13(4). – P. 041302.
15. Liang X., Wang K.K., Zhu T.C. Feasibility of interstitial diffuse optical tomography using cylindrical diffusing fibers for prostate PDT // Physics in Medicine and Biology. – 2013. – Vol. 58(10). – P. 3461–80.
16. Patterson M.S., Madsen S.J., Wilson B.C. Experimental tests of the feasibility of singlet oxygen luminescence monitoring in vivo during photodynamic therapy // J Photochem Photobiol B. – 1990. – Vol. 5(1). – P. 69–84.
17. Filonenko E.V., Saribekyan E.K., Ivanova-Radkevich V.I. Capabilities of Intraoperative Photodynamic Therapy For Treatment Of Locally Advanced Breast Cancer // Biomedical Photonics. – 2016. – Vol. 5, No. 1. – P. 9–14. doi: 10.24931/2413–9432–2016–5–1–9–14.
18. Nakai T., Nishimura G., Yamamoto K., Tamura M. Expression of optical diffusion coefficient in high-absorption turbid media // Phys. Med. Biol. – 1997. – Vol. 42. – P. 2541–2549.
19. Jacques S.L. Optical properties of biological tissues: a review // Phys. Med. Biol. – Vol. 58(11). – P. 37–61.
20. Rendon A., Beck J.C., Lilge L. Treatment planning using tailored and standard cylindrical light diffusers for Photodynamic therapy of the prostate // Phys Med Biol. – 2008. – Vol. 53(4). – P. 1131–1149.

5. Baran T.M., Foster T.H. Comparison of flat cleaved and cylindrical diffusing fibers as treatment sources for interstitial photodynamic therapy, *Med. Phys*, 2014, vol. 41(2), 022701. doi: 10.1118/1.4862078.
6. Farina B., Saponaro S., Pignoli E., Tomatis S., Marchesini R. Monte Carlo simulation of light fluence in tissue in a cylindrical diffusing fiber geometry, *Phys Med Biol*, 1999, vol. 44(1), pp. 1–11.
7. Baran T.M., Foster T.H. New Monte Carlo model of cylindrical diffusing fibers illustrates axially heterogeneous fluorescence detection: simulation and experimental validation, *J Biomed Opt*, 2011, vol. 16(8),085003. doi: 10.1117/1.3613920.
8. Altschuler M.D., Zhu T.C., Li J., Hahn S.M. Optimized interstitial PDT prostate treatment planning with the Cimmino feasibility algorithm, *Med. Phys.*, 2005, vol. 32, pp. 3524–3536.
9. Oakley E., Bellnier D.A., Hutson A., Wrazen B., Arshad H., Quon H., Shafirstein G. Surface Markers for Guiding Cylindrical Diffuser Fiber Insertion in Interstitial Photodynamic Therapy of Head and Neck Cancer, *Lasers Surg Med*, 2017, vol. 49(6), pp. 599–608.
10. *Cylindrical light diffuser Model RD*. Available at: http://www.medlight.com/pdf/Doc_RD_0801E.pdf. (accessed 28.11.2019)
11. Sandell J.L., Zhu T.C. A review of in-vivo optical properties of human tissues and its impact on PDT, *Journal of Biophotonics*, 2011, vol. 4(11–12), pp. 773–87.
12. Dimofte A., Finlay J.C., Liang X., Zhu T.C. Determination of optical properties in heterogeneous turbid media using a cylindrical diffusing fiber, *Physics in Medicine and Biology*, 2012, vol. 57(19), pp. 6025–46.
13. Dimofte A., Finlay J.C., Zhu T.C. A method for determination of the absorption and scattering properties interstitially in turbid media, *Physics in Medicine and Biology*, 2005, vol. 50(10), pp. 2291–311.
14. Jacques S.L., Pogue B.W. Tutorial on diffuse light transport, *Journal of Biomedical Optics*, 2008, vol. 13(4), pp. 041302.
15. Liang X., Wang K.K., Zhu T.C. Feasibility of interstitial diffuse optical tomography using cylindrical diffusing fibers for prostate PDT, *Physics in Medicine and Biology*, 2013, vol. 58(10), pp. 3461–80.
16. Patterson M.S., Madsen S.J., Wilson B.C. Experimental tests of the feasibility of singlet oxygen luminescence monitoring in vivo during photodynamic therapy, *J Photochem Photobiol B*, 1990, vol. 5(1), pp. 69–84.
17. Filonenko E.V., Saribekyan E.K., Ivanova-Radkevich V.I. Capabilities of Intraoperative Photodynamic Therapy For Treatment Of Locally Advanced Breast Cancer, *Biomedical Photonics*, 2016, vol. 5, no. 1, pp. 9–14. doi: 10.24931/2413–9432–2016–5–1–9–14.
18. Nakai T., Nishimura G., Yamamoto K., Tamura M. Expression of optical diffusion coefficient in high-absorption turbid media, *Phys. Med. Biol.*, 1997, vol. 42, pp. 2541–2549.
19. Jacques S.L. Optical properties of biological tissues: a review, *Phys. Med. Biol.*, vol. 58(11), pp. 37–61.
20. Rendon A., Beck J.C., Lilge L. Treatment planning using tailored and standard cylindrical light diffusers for Photodynamic therapy of the prostate, *Phys Med Biol*, 2008, vol. 53(4), pp. 1131–1149.